Indian Journal of Chemistry
Vol. 58A, July 2019, pp. 763-771

# Enhancement of photocatalytic degradation of an organic pollutant by $WO_3$ nanopowders: Carbon doping

Vasanthi Pillay, Gundeboina Ravi & Vithal Muga*

Department of Chemistry, Osmania University, Hyderabad 500 007, Telangana, India

Email: mugavithal@gmail.com

*Received 18 January 2019; revised and accepted 19 June 2019*

The photocatalytic activity of $WO_3$ and C doped $WO_3$ has been monitored by studying the degradation of the methylene blue (MB) aqueous dye solution under visible light irradiation. The photocatalyst $WO_3$ has been synthesized by the solvothermal method and modified by doping carbon into it in the molar ratio 1:1, 1:2, 1:3 and 1:4 under hydrothermal process. The photocatalysts have been characterized for structural and optical properties. XRD has been taken to identify the phase and structure, also confirms the successful incorporation of carbon into $WO_3$ lattice site. Morphology and elemental composition were analyzed using SEM and EDAX. The UV-DRS spectrum showed an increase in absorption intensity with increasing carbon content with decreases in band gap from 3.0 eV to 2.6 eV. PL emission spectra gave blue emission (484 nm) and green emission (555 nm). Finally, the photocatalytic response graph of C doped $WO_3$ with time showed an excellent absorption property and an enhanced visible-light photocatalytic activity compared to pristine $WO_3$.

**Keywords:** Photocatalytic activity, Carbon doped tungsten trioxide, Solvothermal method, Visible light methylene blue degradation

Textile effluent is the cause of a significant amount of environmental degradation and human illnesses. Among the many chemicals that can be found in textile wastewater, dyes are considered as the worst pollutants. Dyes have a synthetic origin and complex aromatic molecular structures which make them more stable and more difficult to biodegrade[1]. The presence of very little amounts of dyes (<1 mg/L for some dyes) in water, which are nevertheless visible seriously affects the aesthetic quality and transparency of water bodies. Some of these dyes are toxic and can cause lung and skin irritations, headaches, congenital malformations and nausea[2]. Therefore, different separation techniques have been used for the treatment of dye-bearing wastewater such as adsorption, coagulation/flocculation, advanced oxidation technologies, ozonation, and membrane-filtration, aerobic and anaerobic degradation. All of these techniques have their own limitations in terms of design, operation efficiency and total cost. In the present study, Advanced Oxidation Process (AOP) is used as the dye degradation technique.

AOPs are efficient methods to remove organic contamination not degradable by means of biological processes. One of the AOP techniques is the heterogeneous photocatalysis, which is based on the generation of highly reactive and oxidizing hydroxyl radicals in the presence of an irradiated semiconductor metal oxide[3]. Semiconductor photocatalysis process can be an appropriate tool for the treatment for textile and printing industry wastewater as it can operate at ambient temperature and pressure with complete mineralization, and low operating cost[4]. Accordingly, $TiO_2$, $ZrO_2$, $KTaO_3$, $SrTiO_3$, and $BiVO_4$ are good candidates for photocatalytic degradation of organic dyes[5-7]. However, most semiconductor catalysts only operate under ultraviolet (UV) light which accounts for only ca. 4% of the total solar energy[8–10]. Visible light activity semiconductors are desirable since the solar light contains almost half of visible light. The band gap of semiconductor materials should be less than 3 eV to have a visible light response. Recently, $WO_3$ is gaining much importance and several researchers are exploring $WO_3$ as an effectively visible light harvesting photocatalyst. Unlike traditional photocatalytic $TiO_2$, which can absorb only ultraviolet (UV) light, $WO_3$ with a band gap between 2.5 and 3.0 eV is considered to be a visible-light-driven semiconductor photocatalyst. The photogenerated

holes in $WO_3$ can oxidize nearly all kinds of organic compounds[11-14]. It is well known that the photocatalytic performance can be improved by doping with cations or anions. Chemical doping of $WO_3$ with metal ions Cu, Sn and Pd[15-17] have been reported to modify the electronic structures of semiconductors as well as their surface properties leading to better visible light absorption. However, compared with Anionic dopants, they are reported to be less efficient concerning stability, photocatalytic activity, and simplicity of the doping process[18]. Photocatalysts with anion doping to obtain the visible light-activated photocatalyst have been reported in last decades[19-23]. However, the studies of carbon anion doping in $WO_3$ are not reported. Herein we present the preparation, characterization and photocatalytic studies of C doped $WO_3$.

## Materials and Methods

### Preparation of absorbents: synthesis of $WO_3$

The sol-gel method, which is very useful for obtaining pure, homogeneous and nano-sized powders, is used as an experimental technique for preparation of $WO_3$ precursor. An important peculiarity of this technique is the possibility to control the kinetics and mechanism of the proceeding chemical reactions. In other words, one can control each step of the sol-gel process which will affect the final desired outcome[24]. Tungsten metal powder (Sigma-Aldrich, 99.9% purity), citric acid, ethylene glycol, hydrogen peroxide (30%) and ammonia (25%) (All SD fine chemicals, 99%) were used as starting materials as received. Briefly, 13 g of tungsten powder was added to a solution containing 300 mL of hydrogen peroxide in an ice bath and left overnight for complete dissolution. A clear solution is formed after the exothermic reaction. The solution was kept for stirring and subsequently, citric acid was added to the solution such that the molar ratio of metal ions to citric acid was 1:2. Under constant stirring, for about 2 h, dilute ammonia was added drop wise to maintain pH of the solution at 7. The above solution was slowly evaporated on a hot plate under constant stirring till a thick, viscous solution was obtained. At this stage, ethylene glycol was added in the molar ratio of citric acid to ethylene glycol as 1:1.2. Finally, the solution was evaporated slowly at 60 °C increasing 5 °C each day until a gel was obtained. The gel was dried to get a black porous solid, which was crushed thoroughly (designated as a precursor) and heated at 500 °C for 4 h to obtain $WO_3$.

### Carbon doping in $WO_3$

C doped $WO_3$ nanoparticles were prepared by the hydrothermal method, taking glucose as the carbon source. The molar ratio of $WO_3$:$C_6H_{12}O_6$ in the reaction mixture was 1:1, 1:2, 1:3, and 1:4. In a typical procedure, a designed amount of $WO_3$ and glucose was dissolved in 60 mL deionized water under continuous stirring at room temperature. After continued mixing for 1 h, the mixture was transferred into a 100 mL Teflon lined autoclave, sealed and heated to 160 °C at 50 °C per hour and kept for 12 h followed by furnace cooling. The obtained brown precipitate was filtered and washed with distilled water and dried overnight at 60 °C.

### Photocatalytic experiment

For this study, methylene blue dye was taken as a model pollutant. The photocatalytic activity studies of all the samples were evaluated by the decomposition of methylene blue aqueous solution under visible light irradiation using a Heber Visible Annular Type Photoreactor, model HVAR1234 (Heber scientific, Chennai, India). A 500 W tungsten lamp (380–840 nm) was positioned inside a cylindrical quartz vessel, and the reaction was carried out at room temperature. Methylene blue solution of the desired concentration (10 mg/L) was prepared using distilled water. In each adsorption experiment, 0.005 g of photocatalyst was added to 50 mL of the dye solution. Prior to the photocatalytic test, the photocatalyst was suspended in an aqueous solution of methylene blue dye and air was bubbled through the mixture and stirred for 60 min in the dark to establish the adsorption-desorption equilibrium between the dye and catalyst. Now, the solution is irradiated with visible light for the commencement of the photocatalytic reaction. At different time intervals, samples from the mixture were taken out, filtered and subjected to absorbance measurements. The absorbance of the samples was analyzed using a UV-Vis spectrophotometer. The degradation amount of dye was calculated from the equation

$$D = \left(\frac{C_0 - C}{C_0}\right) \times 100\%$$

Here $D$ is the percentage of degradation, $C_0$ initial concentration of dye and $C$ was the concentration at time $t$.

### Characterization techniques

In order to understand the structure and the phase of the catalysts, the X-ray diffraction (XRD) patterns

were recorded using Rigaku, D/Max II X-ray diffractometer. The X-ray radiation source used is Cu Kα radiation (λ = 0.154 nm). Information about the elemental composition and the morphological characterization was obtained from EDS and SEM measurements. The absorption and emission of the photon by the dye solution was studied using photoluminescence spectroscopy. UV-Vis-DRS were recorded on a spectrophotometer equipped with an integrating sphere and using $BaSO_4$ as a blank reference. The band gap energy was calculated from the Tauczation of the plot, using the Kubelka–Munk function from the reflectance measurements.

## Results and Discussion

### Structural analysis

The XRD of a compound is its 'fingerprint' and can be used to identify it. The 2θ angles at which the peak intensities occur (Fig. 1) are related to the inter-planar distances of the atomic structure and are related by Bragg's law:

$$n\lambda = 2d \sin\theta$$

Where λ is the wavelength of X-ray radiation used, θ is the peak position angle and d is the inter-planar distance.

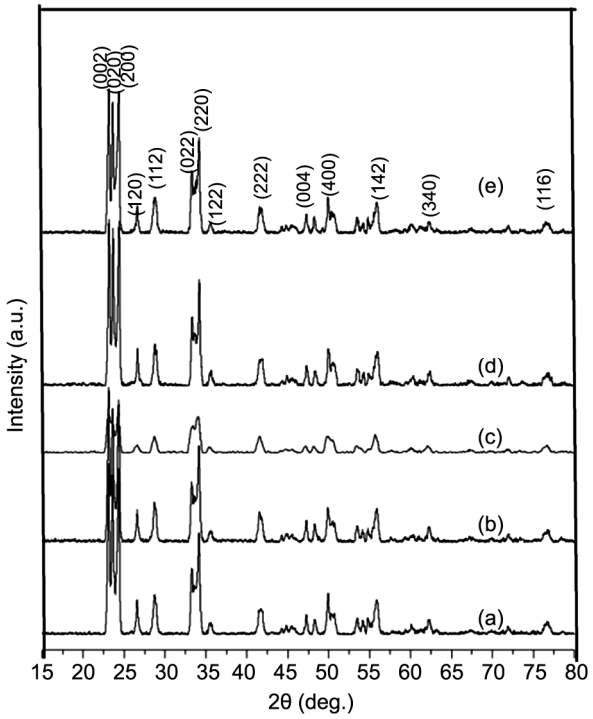


Fig. 1 — XRD profiles of $WO_3$ and C doped $WO_3$ of different molar ratio of C in $WO_3$ (a) $WO_3$, (b) $WO_3$: C-1:1, (c) $WO_3$:C-1:2, (d) $WO_3$: C -1:3, and, (e) $WO_3$: C -1:4.

In a polycrystalline sample the full width at half maximum (FWHM) of a peak can be related to the average crystallite size of sample. The crystallite size, D, of samples from the XRD data at 2θ = 24° is found to be 18 nm for $WO_3$ and 23, 20, 30 and 25 nm, for the $WO_3$ doped with carbon, in the molar ratio of 1:1, 1:2, 1:3 and 1:4 respectively. The variation in the grain size can be attributed to the lattice distortion introduced in the system due to doping. The estimate excludes the effects of peak broadening due to the instrument used and any effect of residual stresses. The diffractograms of the pristine $WO_3$ and the C doped $WO_3$ confirmed monoclinic structure lattice, with no additional impure phase. All the diffraction peaks matched well with the JCPDS data (83-0951) reported for this material. This shows that the incorporation of carbon into $WO_3$ does not introduce any change in the main crystal system. When the XRD patterns are plotted in an expanded scale (Fig. 2), a shift in the diffraction peak position is noticed towards lower 2θ values indicating the incorporation of C into $WO_3$ lattice. The lattice parameters of the parent $WO_3$ and C doped $WO_3$ are evaluated and given in Table 1. As observed from the table the lattice

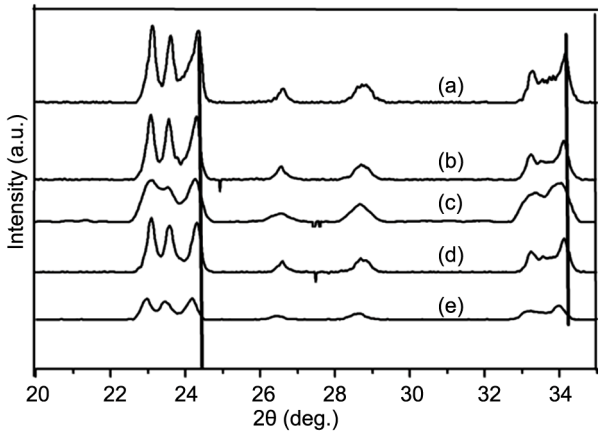


Fig. 2 — XRD profiles of $WO_3$ and C doped $WO_3$ in expanded scale showing shift in peak position toward lower 2θ (a) $WO_3$, (b) $WO_3$: C-1:1, (c) $WO_3$: C-1:2, (d) $WO_3$: C -1:3, and, (e) $WO_3$: C -1:4.

Table 1 — Lattice parameters of pristine $WO_3$ and C doped $WO_3$

| Doping concentration (% wt) | Lattice parameter a (Å) | Lattice parameter b (Å) | Lattice parameter c (Å) | Volume V($cm^3$) |
|---|---|---|---|---|
| 1: 0(pristine $WO_3$) | 7.2889 | 7.5348 | 7.6971 | 422.69 |
| 1:1 | 7.2988 | 7.5409 | 7.6872 | 423.06 |
| 1:2 | 7.3058 | 7.5427 | 7.6932 | 423.93 |
| 1:3 | 7.3018 | 7.5499 | 7.6953 | 424.21 |
| 1:4 | 7.3074 | 7.5561 | 7.7035 | 425.33 |

parameters *a, b, c* varies in a disordered manner, with the variation in the doping concentration. The unit cell volume of C doped $WO_3$ increased compared to the parent $WO_3$. The observed variation in lattice parameters and the unit cell volume is consistent with the fact of C anion (2.6 Å) having a bigger radius than $O^{2-}$ (1.22 Å) radius. Hence the volume of the unit cell expands with the increase in the doping concentration, and this confirms the doping of C into $WO_3$ lattice.

**SEM**

Scanning Electron Microscopy (SEM) is a useful technique to determine the morphology and particle size of the materials. SEM images of parent and C doped $WO_3$ in different molar ratio is shown in Fig. 3. It is seen that both the pristine and C doped $WO_3$ samples have granular morphology, suggesting that doping of $WO_3$ does not affect the structure, crystallinity or morphology of the compound. As the doping ratio increased the grains begin to agglomerate, which is consistent with the calculated grain size from XRD data which shows an increase in the grain size and increasing disorderness, as the doping concentration increases. The surface composition of C doped $WO_3$ is determined by Energy Dispersive Spectroscopy (EDS). The merged EDS spectra of pure and C doped $WO_3$ at different molar ratio is shown in Fig. 4. The surface of the $WO_3$ nanoparticles exhibited elements of W, O and C. The atomic ratio of W/O/C is shown in Table 2. The calculated stoichiometry ratio from the EDS measurements is consistent with the initial precursor, which had been taken for the synthesis process.

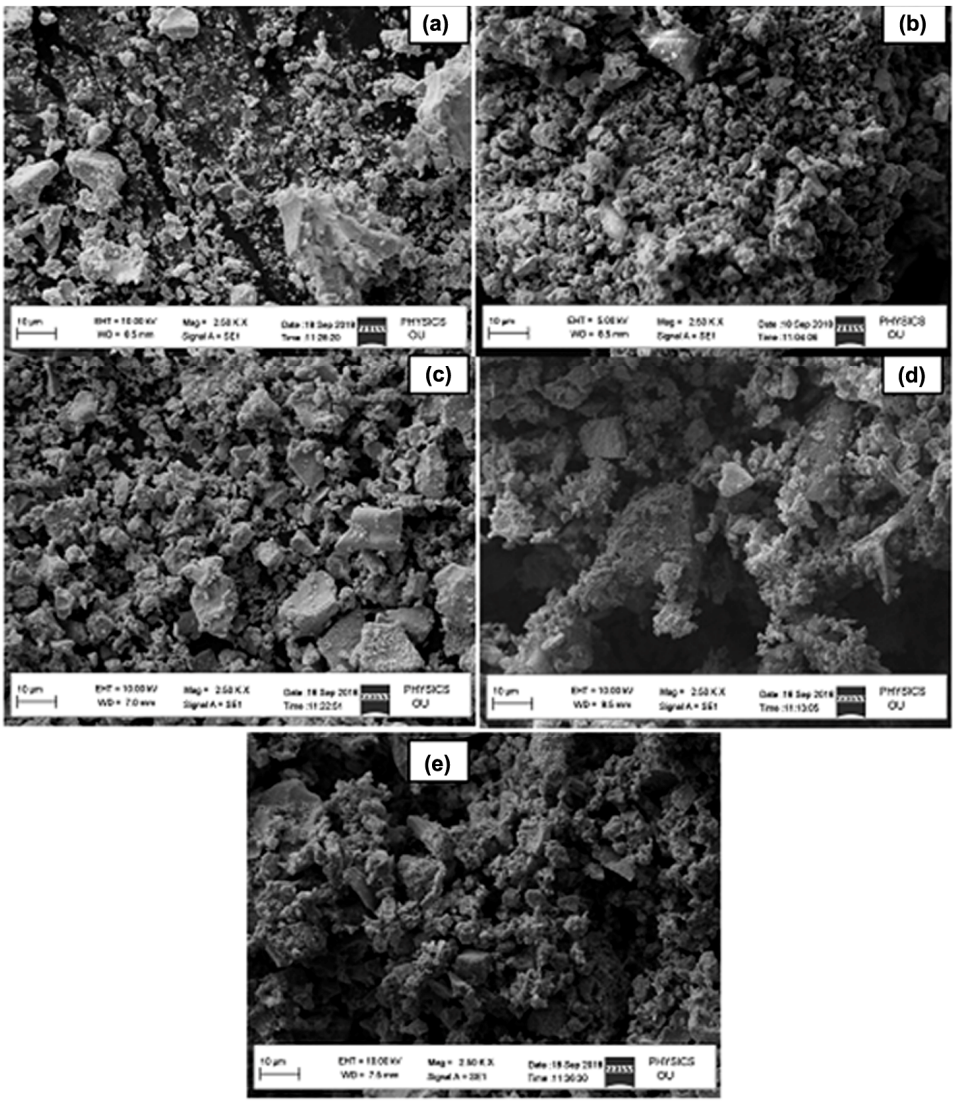


Fig. 3 — SEM images of $WO_3$ and C doped $WO_3$ (a) $WO_3$, (b) $WO_3$: C-1:1, (c) $WO_3$: C-1:2, (d) $WO_3$: C -1:3, and, (e) $WO_3$: C -1:4.

**Optical studies**

Diffuse reflectance spectroscopy (DRS) is a reliable and efficient tool for the analysis of optical parameters of materials. The absorption edge and band gap energies of the parent $WO_3$ and C doped $WO_3$ are investigated based on the onset of the absorption spectra. UV-DRS spectra of the pristine and C doped $WO_3$ samples are shown in Fig. 5. Based on the reflectance spectra the absorption edge for each compound was determined. Using the absorption edge values the band gap energy was calculated (Fig. 6) in each case and is shown in Table 3. As observed from the table the absorption edge of the samples increases with the doping ratio from 1:1 to 1:3, a shift in the absorption edge towards longer wavelength is seen. However for the 1:4 ratios sample the absorption intensity decreases. Also, the band gap energies for the doped samples are calculated to be lower than pristine $WO_3$ to the doped samples. Generally, the change in the band gap energy of the compound occurs due to the modification of the density of energy state due to change in the chemical

Table 2 — Elemental analysis of pristine $WO_3$ and C doped $WO_3$

| Compound | Tungsten (W) | | Oxygen (O) | | Carbon (C) | |
|---|---|---|---|---|---|---|
| | Weight (%) | Atomic (%) | Weight (%) | Atomic (%) | Weight (%) | Atomic (%) |
| $WO_3$:C-1:0 | 75.69 | 19.88 | 17.57 | 53.04 | 6.74 | 27.08 |
| $WO_3$:C-1:1 | 67.27 | 13.21 | 15.42 | 34.78 | 17.31 | 52.01 |
| $WO_3$:C-1:2 | 55.44 | 8.17 | 15.52 | 26.29 | 29.04 | 65.53 |
| $WO_3$:C-1:3 | 40.71 | 4.71 | 21.97 | 29.21 | 37.32 | 66.08 |
| $WO_3$:C-1:4 | 24.41 | 2.24 | 23.85 | 25.13 | 51.75 | 72.64 |

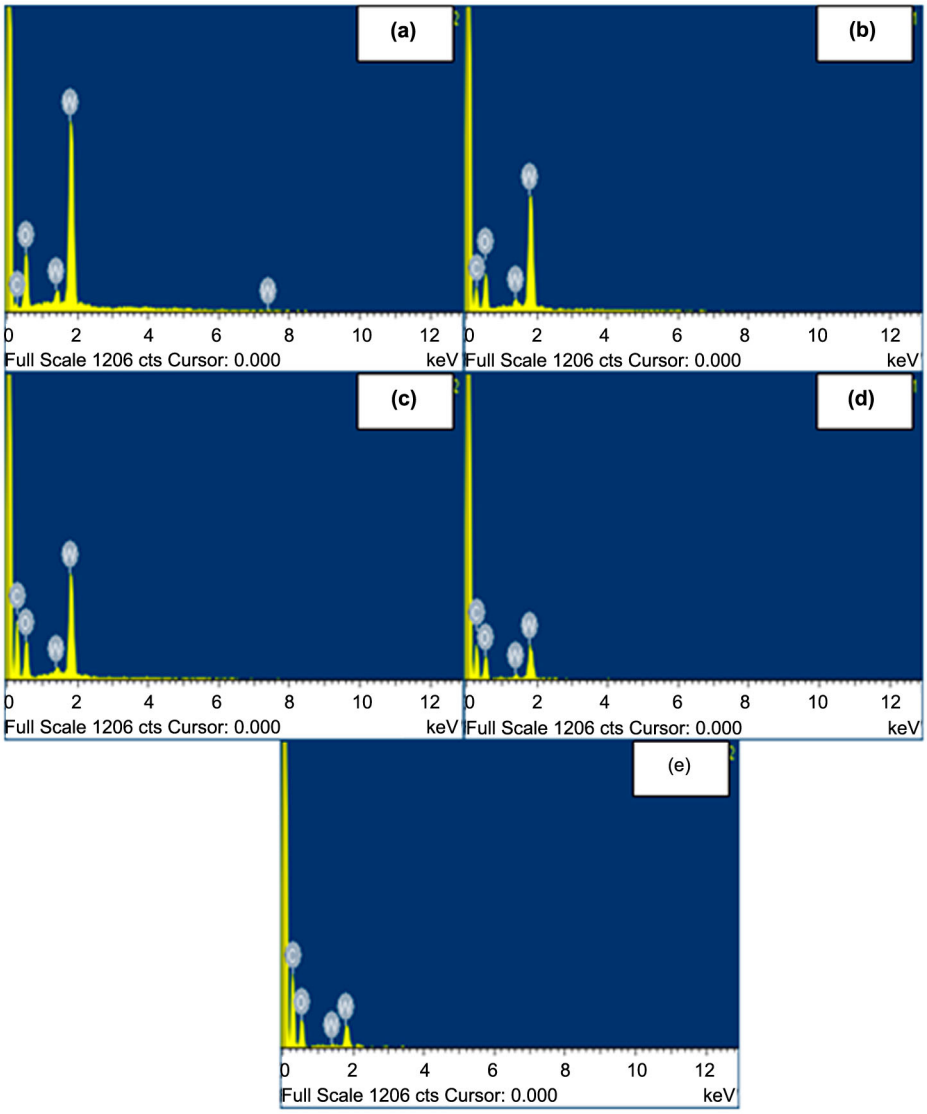


Fig. 4 — EDS images of Carbon in C doped $WO_3$, (a) $WO_3$, (b) $WO_3$: C-1:1, (c) $WO_3$: C-1:2, (d) $WO_3$: C -1:3, and, (e) $WO_3$: C -1:4.

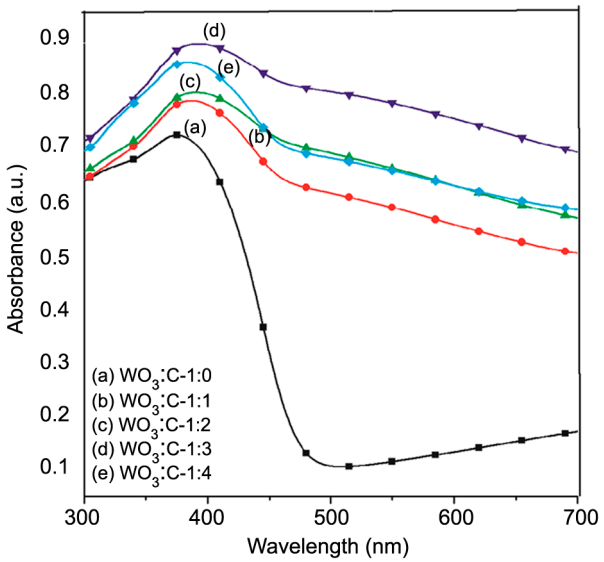


Fig. 5 — The diffuse reflectance spectrum of $WO_3$ and C doped $WO_3$ at different molar ratio.

Table 3 — Optical parameters of pristine $WO_3$ and C doped $WO_3$

| Compound | Absorption edge (nm) | Energy band gap (eV) |
|---|---|---|
| $WO_3$ | 415 | 3.0 |
| $WO_3$:$C_{1:1}$, | 478 | 2.6 |
| $WO_3$:$C_{1:2}$, | 540 | 2.3 |
| $WO_3$:$C_{1:3}$ | 622 | 2.0 |
| $WO_3$:$C_{1:4}$ | 478 | 2.6 |

composition of the material; The observed decrease in band gap energy of the C doped samples, can be attributed to the formation of localized states in the band gap of $WO_3$ due to carbon doping, confirming that the carbon has gone into the lattice site of the $WO_3$ as evident from the XRD studies.

**Photoluminescence studies**

Photoluminescence (PL) spectroscopy is an efficient optical method to probe the electronic structure of materials. The PL spectrum at room temperature shows the spectral peaks associated with impurities in the parent material. The reasonably high sensitivity of this technique provides the potential to identify extremely low concentrations of intentional and unintentional impurities that can strongly affect the material quality and device performance. A PL spectrum is a measure of the intensity of radiation versus wavelength emitted as a result of radiative recombination of electron-hole pairs or excitons from their thermal equilibrium states by optical excitation[25]. Photoexcitation of a semiconductor material promotes an electron from the valence band

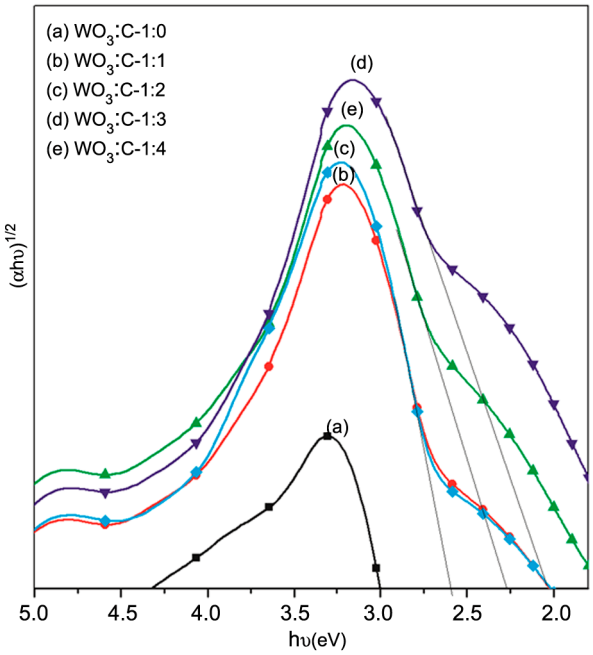


Fig. 6 — Plot of $(\alpha h\upsilon)^{1/2}$ vs hυ plot for $WO_3$ and C doped $WO_3$ at different molar ratio.

(VB) to the conduction band (CB), leaving a 'hole' in the VB. The excited electron in the CB relaxes quickly, typically within 15–25 ps, to the band edge via inter or intra sub-band scattering and then recombines with the hole either radiatively by emitting a photon or non-radiatively by passing the energy on to one or more photons, to 'trapping' states that are created by impurities, dopants or defects and lie in between the conduction band and the valence band (Shockley–Read–Hall recombination)[26,27], or to another electron or hole (Auger recombination)[28] . PL emission spectra of pure and C doped $WO_3$ samples are shown in Fig. 7. Both the pure and doped samples show blue emission (484 nm) and green emission (555 nm). In general, the visible region PL emission in $WO_3$ is expected to arise due to surface defects and oxygen vacancies developed in shallow and deep trap states. These intrinsic defect states act as active centres in luminescence processes[29,30]. The blue and the green emissions are due to the interstitial defects resulting from non-stoichiometric $WO_3$ and surface defects of oxygen vacancies related to F or $F^{2+}$ color centers respectively. During doping, the energy levels increases, resulting in the reduction of the band gap. The doped element acts as an electron sink and thereby results in the suppression of electron-hole recombination due to the shorter distance of interband metal ions, which result in an energy transfer between

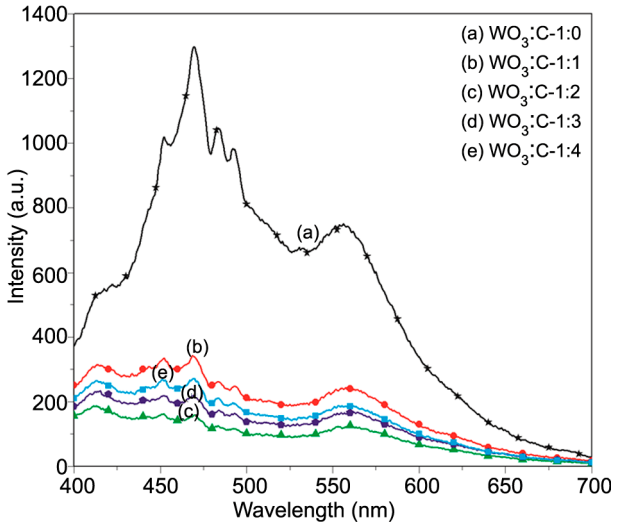


Fig. 7 — Photoluminescence spectrum of $WO_3$ and C doped $WO_3$ different molar ratio.

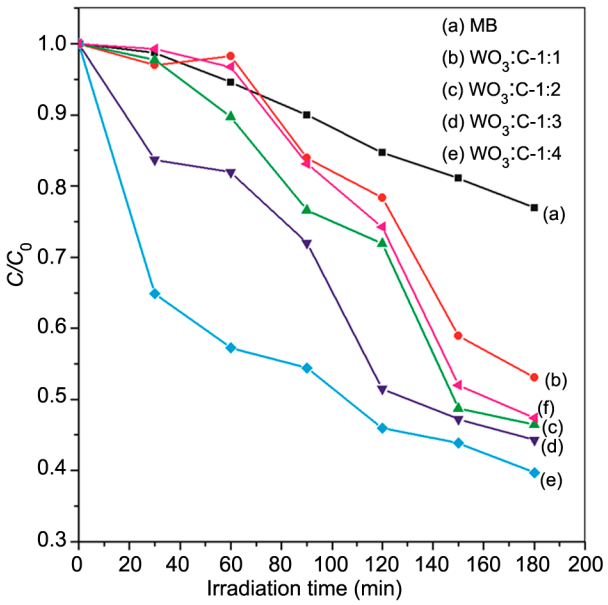


Fig. 8 — Photocatalytic degradation curves of MB, $WO_3$ and C doped $WO_3$ for different molar ratio.

nearby ions. In this case, fewer electrons would come back to the valence band and would emit lesser energy in the form of light. Therefore, a concentration quenching process will occur, which result in a non-radiative decay process due to which PL intensity decreases and peaks are broader as seen in Fig. 7. There exists a relationship between band gap and PL intensity and the DRS results are consistent with the PL spectra. The C doped $WO_3$ states promote absorption whose tail extends deep into the forbidden gap, and thereby the narrower band gap of $WO_3$ occurs.

**Photocatalytic activity**

To study the photocatalytic activity of the samples, they are irradiated with photons of visible light in the presence of MB dye solution. Comparison of photocatalytic degradation of MB as a function of irradiation time for all the samples with different doping ratio is shown in Fig. 8. The photocatalytic activity of pure MB, pristine $WO_3$ and C doped $WO_3$ were measured and a graph is plotted between the amount of degradation of dye and the irradiation time. It is evident from Fig. 8 that only 23% of MB is degraded in 180 min under visible light illumination, in the absence of a catalyst. Thus, the photolysis of MB is negligible. In the presence of catalyst $WO_3$, the degradation increased up to 47%. For the catalyst doped with carbon in the molar ratio of 1:1, 1:2 and 1:3, degradation of dye was observed to be 54%, 56% and 60% respectively. Dependence of photocatalytic activity on catalyst doping with carbon is given in Table 4. It is interesting to see that, as the amount of C doping increased, the photocatalytic activity also increased. According to the literature it is understood that incorporation of the carbon could improve the photocatalyst efficiency in semiconductor in the following way: (i) band gap narrowing[31], (ii) formation impurity energy levels[32], (iii) creating oxygen vacancies, (iv) creating a unique surface area for the adsorption of organic molecules[21] and (v) electron trapping[33]. In general, the photocatalytic activity of prepared catalyst depends well on how recombination of photo-induced electron-hole pairs is avoided. Doping prevents recombination of the electrons and the holes and gets better photocatalytic activity by trapping the photo-induced electrons[34-36]. The positively charged holes are potent oxidants and can destroy adsorbed organic pollutants whereas the electrons at the conduction band react with the dissolved oxygen molecules to form strong oxidative

Table 4 — Photo catalytic activity of $WO_3$ and C doped $WO_3$

| Catalyst | Loading Conc$^n$ (wt %) | Organic pollutant | Irradiation time (min) | Degradation efficiency (%) |
|---|---|---|---|---|
| None | 0 | Methylene Blue | 180 | 23 |
| $WO_3$ | 1:0 | Methylene Blue | 180 | 47 |
| $WO_3$:C | 1:1 | Methylene Blue | 180 | 54 |
| $WO_3$:C | 1:2 | Methylene Blue | 180 | 56 |
| $WO_3$:C | 1:3 | Methylene Blue | 180 | 60 |
| $WO_3$:C | 1:4 | Methylene Blue | 180 | 53 |

radicals ($O_2^-$) that also cause the decomposition of organic and inorganic contaminations in wastewater[37]. However, the photoactivity of 1:4 molar ratio of $WO_3$:C is reduced to 53%. According to literature beyond the optimum amount of catalyst loading, with increasing the doping concentration increases the opacity of the solution, and thus increasing the light scattering and the infiltration depth of the photons is diminished and less amount of photocatalysts could be activated[38,39]. Hence, results in the reduction of the degradation rate which is consistent with the result shown by the PL graph, with a decrease in the peak intensity.

## Conclusions

In summary, it may be concluded that tungsten trioxide ($WO_3$) semiconductor plays a notable role in the field of photocatalysis. While a vast range of $WO_3$ nanostructures has already been reported in the literature, it is still very important to continue the exploration of innovative synthesis routes of nanostructured $WO_3$, as well as to investigate the mechanism of growth control. The pristine and C doped $WO_3$ nanoparticles have been successfully prepared by simple sol-gel technique and doping was done by hydrothermal method. Powder XRD results reveal $WO_3$ and C doped $WO_3$ crystallized with monoclinic lattice and the results are in good agreement with the standard JCPDS data (card no: 83-0951). SEM images showed granular morphology with average particle size around 18–25 nm. C doping into the $WO_3$ reduces the band gap as evident by a blue shift in the optical absorption edge in the UV-Vis spectra. In addition, UV and PL results suggested that photoabsorption of C doped $WO_3$ was in the visible-light region. This could be attributed that C dopant introduced the emergence of a new level above the valence band of $WO_3$, leading to narrow band gap and enhancing the visible-light absorption. The change of band structure, distortion of $WO_3$ lattice and lattice defects due to carbon doping helps to improve the photocatalytic performance of C doped $WO_3$ as compared with pristine $WO_3$ in the degradation of MB under visible light irradiation.

## Acknowledgement

The authors are thankful to the Department of Science and Technology, Government of India for financial support vide (reference no: SR/WOS-A/PM-111/2016) under Women Scientist Scheme to carry out this work.

## References

1 Aksu Z, *Process Biochem,* 40 (2005) 999.
2 Mathur N, Bhatnagar P & Bakre P, *Appl Ecol Env Res,* 4 (2005) 111.
3 Carp O, Huisman C L & Reller A, *Prog Solid State Chem,* 32 (2004) 33.
4 Chong M N, Jin B, Chow C K W & Saint C, *Water Res,* 44 (2010) 2997.
5 Halmann M & Grätzel M, *Energy Resources through Photochemistry and Catalysis,* (Academic press, United States), 1983.
6 Serpone N & Pelizzetti E, *Photocatalysis: Fundamentals and Applications*, (Wiley, New York), 1989.
7 Pleskov Y V & Gurevich Y Y, *Semiconductor Photoelectrochemistry*, (Springer, New York), 1986.
8 Kudo A & Miseki Y, *Chem Soc Rev,* 38 (2009) 253.
9 Linsebigle A L, Yates J T, Jr & Lu G, *Chem Rev,* 95 (1995) 735.
10 Zou Z, Ye J, Sayama J & Arakawa H, *Nature,* 414 (2001) 625.
11 Irie H, Miura S & Kamiya K, *Chem Phys Lett,* 457 (2008) 202.
12 Kikuchi M, Imai M, Miyamura A, Sato Y & Shigesato Y, *Proceedings of the 6th International Conference on Coatings on Glass and Plastics*, (Germany), (2006) 365.
13 Abe R, Takami H, Murakami N & Ohtani B, *J Am Chem Soc,* 25 (2008) 7780.
14 Bamwenda G R, Sayama K & Arakawa H, *J Photochem Photobiol A,* 122 (1999) 175.
15 Bai X, Ji H, GoaP, Zhang Y & Sun X, *Sens Actuat B: Chem*, 31(2014) 100.
16 Upadhyay S B, Mishra R K & Sahay P P, *Sens Actuat B: Chem*, 193(2014) 19.
17 Hua Z, Yuasa M, Yamazoe T & Shimanoe K, *Thin Solid films,* 548 (2014) 677.
18 Ghaffari M, Huang H, Tan P Y & Tan O K, *Powder Technol,* 225 (2012) 221.
19 Ananpattarachai J, Kajitvichyanukul P & Seraphin S, *J Haz Mater,* 168 (2009) 253.
20 Sobana N, Muruganandam M V & Swaminathan M S, *Catal Comm,* 9 (2008) 262.
21 Wu Y, Xing M, Tian B, Zhang J & Chen F, *Chem Eng J*, 162(2010) 710.
22 Morikawa T, Asahi R, Ohwaki T, Aoki K, Suzuki K & Taga Y, *R&D Review of Toyota CRDL,*40 (2005) 45.
23 Sakthivel S & Kisch H, *Angew Chem Int Ed Engl,* 42 (2003) 4908.
24 Dimitriev Y, Ivanova Y & Iordanova R, *J Univ Chem Techn Metall,* 43(2008) 181.
25 Nishino T, Nakayama H & Hamakawa Y, *Japan Annual Reviews in Electronics, Computers and Telecommunications Semiconductor Technologies*, North+ Holland NY 8 (1985) 295.
26 Shockley W & Read W T, *Phys Re*v, 87 (1952) 835.
27 Hall R N, *Phys Rev,* 83 (1951) 228.
28 Haug A, *J Phys c: solid state Phys,* 16 (1983) 4159.
29 Mathew S, Prasad A K, Benoy T, Rakesh P P, Hari M, Libish T M, Radhakrishnan P, Nampoori V P & Vallabhan C P, *J Fluoresc,* 22 (2012)1563.
30 Mattioli G, Filippone F, Alippi P & Bonapasta A M, *Phys Rev B,* 78 (2008) 241201.

31 Sathishkumar P, Mangalaraja R V, Anandan S & Kumar A, *Chem Eng J,* 220 (2013) 302.
32 Cao Y, Yu Y, Zhang P & Zhang L, *Sep Purif Technol,* 104 (2013) 256.
33 Barakat N A M, Kanjwal M A, Chronakis I S & Kim H Y, *J Mol Catal A: Chem,* 366 (2013) 333.
34 Liu Y, Ohko Y, Zhang R, Yang Y & Zhang Z, *J Haz Mater,* 184 (2010) 386.
35 Lin H Y, Chen Y F & Chen Y W, *Int J Hydr Ener,* 32(2007) 86.
36 Zhang Q, Wang H & Li Y, *J Haz Mater,* 254 (2013) 318.
37 Cao M, Lin J, Lu J, You Y & Liu T, *J Haz Mater,* 186 (2011) 948.
38 Seshadri H, Chitra S, Paramasivan K & Sinha, P K, *Desalination,* 232 (2008) 139.
39 Pouretedal H R, Norozi A, Keshavarz M H & Semnani A, *J Haz Mater,* 162 (2009) 674.